Journal of Nuclear Materials 540 (2020) 152371

Contents lists available at ScienceDirect

Journal of Nuclear Materials

journal homepage: www.elsevier.com/locate/jnucmat

Electronic stopping in molecular dynamics simulations of cascades in 3C–SiC

Eva Zarkadoula [a, *], German Samolyuk [a], Yanwen Zhang [a], William J. Weber [a, b]

[a] Materials Science & Technology Division, Oak Ridge National Laboratory, Oak Ridge, TN, 37831, USA
[b] Department of Materials Science & Engineering, University of Tennessee, Knoxville, TN, 37996, USA

ARTICLE INFO

Article history:
Received 12 March 2020
Received in revised form
22 June 2020
Accepted 29 June 2020
Available online 15 July 2020

Keywords:
Radiation damage
Silicon carbide
Molecular dynamics
Electronic stopping
Electronic effects

ABSTRACT

We investigate the effect of the electronic stopping power on defect production due to ion irradiation of cubic silicon carbide using molecular dynamics simulations. We simulate 20 keV and 30 keV Si and C ions, with and without the electronic energy loss. The results show that the electronic stopping effects are more profound in the case of C irradiation, where the ratio of the electronic energy loss S_e to the nuclear energy loss S_n is much larger compared to the ratio for Si ions. These findings indicate that this ratio plays a role in the effect of the electronic stopping on ion irradiation.

Published by Elsevier B.V.

1. Introduction

Silicon carbide, SiC, is an important material for nuclear, high temperature and electronic applications. Due to its high thermal conductivity, chemical stability and good radiation response it has been studied extensively [1–5]. A number of molecular dynamics (MD) studies on primary radiation damage in SiC [6–12] have given useful information on defect production and clustering in SiC. *Ab initio* and MD simulations in SiC have been used to investigate diffusion mechanisms and energy barriers, and a number of studies have looked into defect and cluster evolution and growth [13–20].

In this work, we investigate the effect of the electronic stopping on intermediate energy ion irradiation in cubic SiC. For low energy irradiation events, the energy transfer to the target material happens primarily via the nuclear stopping power. For intermediate energy events, the energy loss from the projectile is partitioned between transfer to the nuclei of the target material and to the electrons. The energy transfer to electrons takes place via the electronic energy loss. While the nuclear energy loss results in defects and defect clusters though collision cascades, the energy loss to the electrons results in the slowing down of atoms that are moving with velocity above a certain cut-off. In other words, this stopping power, the electronic stopping, is the result of the interaction of the projectile with the electrons. Work on metallic systems [21–26] has shown that the electronic stopping affects the number of surviving defects and defect clustering. The effects of the electronic stopping are becoming more understood in metallic systems. However, recently, there have been efforts for better understanding of these effects in band gap materials [27–31]. Additionally, it has been previously shown that the electronic stopping in high energy radiation damage MD simulations in cubic zirconia [32], an insulating material, results in a smaller number of defects and smaller damage range. While the effect of the electronic stopping has been investigated in metallic systems, there is no systematic investigation of the electronic stopping in bandgap materials and these effects are not well understood. With this study, we aim to show the significance of taking into account the electronic stopping, as a fundamental process that takes place in primary radiation damage, which is being ignored. Here, we investigate the effect of the electronic stopping on the number of surviving defects in 20 keV and 30 keV Si ion and C ion cascades in SiC, by performing MD simulations with and without the electronic stopping taken into account.

* Corresponding author.
E-mail address: zarkadoulae@ornl.gov (E. Zarkadoula).

https://doi.org/10.1016/j.jnucmat.2020.152371
0022-3115/Published by Elsevier B.V.

2. Simulation methods

For the MD simulations, we used the Large-scale Atomic/Molecular Massively Parallel Simulator (LAMMPS) [33] code. While most commonly a Tersoff interatomic potential for SiC [34] and a modified embedded atom method (MEAM) interatomic potential have been used [35], we used the Gao-Weber interatomic potential [36] joined to the ZBL (Ziegler-Biersack-Littmark) [37] repulsive potentials for short distances [38]. A recent study of Samolyuk et al. [38], which compares these three potentials, demonstrated that the Gao-Weber potential (joined with ZBL potentials for short distances) provides a more realistic description of cascades in SiC. The Gao-Weber potential is based on the Brenner potential formalism [39], which is based on the Tersoff potential and includes additional parameters to account for the chemical environment of the atoms.

The systems have size 541 Å × 541 Å × 541 Å and periodic boundaries. Prior to irradiation, the systems' energy was minimized, and consequently the systems were equilibrated in the isothermal – isobaric ensemble (NPT) ensemble at 300 K for 50 ps, using 1 fs timestep. For the irradiation, 20 keV and 30 keV Si and C primary knock-on atoms (PKA) were used. We performed fifteen irradiation simulations for each PKA for each irradiation condition, with and without electronic stopping, at random velocity directions, using a variable timestep, which evolves with the dynamics of the system during the cascade formation and system relaxation, with a maximum value of 1 fs. The timestep is reset so no atom moves further than a distance of 0.1 Å based on current atom velocities and forces, between 10^{-5} ps and 10^{-3} ps. The same fifteen velocity directions are used in the simulation set with and without electronic stopping. The PKAs are initiated near the (0,0,0) corner of the MD box, directed towards the center of the box. The irradiation simulations without electronic stopping were performed in the microcanonical (NVE) ensemble. To include the electronic stopping in the irradiation simulations, the two-temperature model [40,41] algorithm within LAMMPS was used, which includes the electronic stopping and the electron-phonon interactions in simulations of ion irradiation. The two-temperature model consists of two parts: a) the electronic stopping and b) the electron-phonon interactions. Here, we only use the electronic stopping mechanism and do not activate the electron-phonon coupling energy transfer. The electron-phonon interactions in bandgap materials are more complex compared to metallic materials, as it is more difficult to excite electrons. Therefore, unless very large energies are used, i.e. large enough to excite the electrons, the two-temperature model in its current implementation is not appropriate for describing electron-phonon interactions in bandgap materials, such as SiC. For the electronic stopping, a modified equation of motion is used (Eq. (1)) to calculate the atom trajectories and forces:

$$m_i \frac{\partial \mathbf{v}_i}{\partial t} = \mathbf{F}_i(t) - \gamma_s \mathbf{v}_i \tag{1}$$

where m_i and $\mathbf{v}_i$ is the mass and the velocity of atom i and γ_s is the electronic stopping parameter. The electronic stopping has the form of a friction term in the equation of motion and it is applied only to atoms with velocities larger than a specified cut-off v_0. Therefore, the energy loss of an atom with velocity $\mathbf{v}_i$, because of the electronic stopping during $\Delta(t)$, is (Eq. (2)):

$$\Delta U_i = \gamma_s v_i^2 \Delta(t) \tag{2}$$

Then, the energy loss of the atoms with kinetic energy in the lattice due to the electronic stopping is (Eq. (3)):

$$\Delta U_l = \Delta(t) \sum_i \gamma_s v_i^2 \tag{3}$$

where the sum is over the atoms that move with velocity larger than the cut-off velocity. In metals, the cut-off velocity is assumed to correspond to 10 eV [42] or to energy twice the cohesive energy of the system [40,43]. For insulators, it has been shown that the cut-off energy is related to the band gap of the material [27,28]. In our simulations, we have used cut-off velocity that corresponds to an energy twice the band gap, similar to previous work [32]. The relaxation time for the electronic stopping is $\tau_s = \frac{m_i}{\gamma_s}$ and can be calculated based on the electronic stopping power, S_e, obtained from "The Stopping and Range of Ions in Matter" (SRIM) code [44]. For 20 and 30 keV Si ions in SiC, τ_s was calculated to be 0.40 ps, while for 20 and 30 keV C ions in SiC, τ_s is 0.29 and 0.28 ps, respectively. Both the S_e and S_n values are obtained from the stopping and range tables of the SRIM code.

For the defects analysis, the Wigner-Seitz method was used, and for the cluster analysis the second nearest neighbor criterion is used [12,13,19].

3. Results and discussion

Fig. 1 (a) and (b) show the average number of total defects, the average number of Si defects and the average number of C defects, as the sum of interstitials and vacancies, in SiC due to 20 keV and 30 keV Si PKAs, respectively. The defect count both in cascades with and without electronic stopping is presented. The error bars represent the standard error over fifteen cascade events. For 30 keV Si ion cascades, the effect of the electronic stopping in the defect production is becoming more apparent, with the total number of defects for 30 keV Si in SiC decreased when the electronic stopping is applied. The difference between the Si defects with and without electronic stopping is small, while the electronic stopping seems to affect more the C atom defect production. Overall, for both energies,

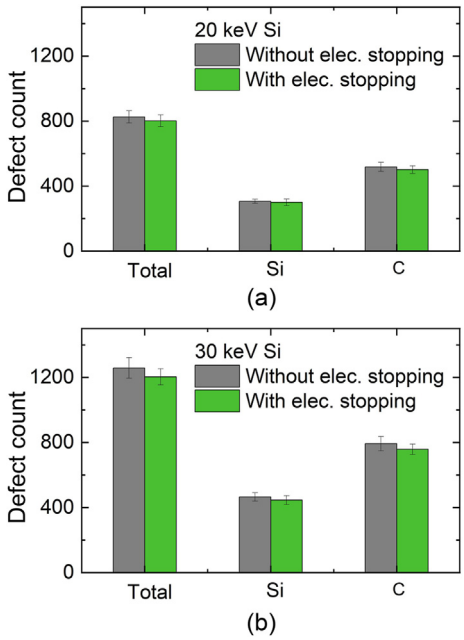

Fig. 1. Average number of defects as sum of interstitial and vacancies in (a) 20 keV Si and (b) 30 keV Si PKA cascades in SiC. The total number of defects and the defects for each atom species are given for cascades with and without electronic stopping. The error bars represent the standard error over fifteen cascade events.

and in both irradiation cases, the number of C defects is about 1.7 times the number of Si defects due to the smaller threshold displacement energy for C atoms compared to Si atoms [8].

In Fig. 2 (a) and (b), the surviving number of interstitials and vacancies for the two different species of atoms are presented, for 20 keV and 30 keV Si PKAs, for cascades with and without electronic stopping. The silicon interstitials and vacancies are noted as Si_{int} and Si_{vac}, respectively. C_{int} and C_{vac} are used for the carbon interstitials and vacancies, respectively. For the 20 keV Si cascades, the electronic stopping does not affect the Si_{int} and Si_{vac}, while the C_{int} and C_{vac} values seem to be more sensitive to the electronic stopping. This can be seen more clearly in Fig. 2 (b), where the number of carbon interstitials and vacancies, C_{int} and C_{vac}, produced in 30 keV Si cascades is smaller when the electronic stopping is applied, compared to cascades where the energy transfer to the electrons is ignored. The effect of the electronic stopping on the silicon interstitials Si_{int} produced in 30 keV Si cascades is small, while at this energy, the electronic stopping affects more the number of Si_{vac} vacancies.

The number of defects produced in 20 keV and 30 keV C PKA cascades are shown in Fig. 3 (a) and (b). Here, the average number of total defects, the average number of Si defects and the average number of C defects in SiC due to 20 keV and 30 keV C ions are shown, respectively, for cascades, both with and without electronic stopping. As seen in Fig. 3 (a), the electronic stopping results in a smaller number of defects in 20 keV C ion cascades. As the energy increases, the effect of the electronic stopping on the number of defects at the end of the cascade is more profound, as seen in Fig. 3 (b). This is consistent with previous studies on the effects of the electronic stopping on the number of surviving defects [21,22,32,45].

The number of silicon interstitials Si_{int} and silicon vacancies Si_{vac} and the number of carbon interstitials C_{int} and carbon vacancies C_{vac} in 20 keV and 30 keV C ion cascades in SiC, with and without electronic stopping, are shown in Fig. 4 (a) and (b). For both 20 keV and 30 keV ion energy, the electronic stopping has a larger effect on the number of carbon defects, both the C_{int} and C_{vac}, compared to the silicon defects. We observe that the error bars overlap more for the carbon ions. Even though we have avoided low defect density directions, the ion energies used here result in formation of more subcascades for C, which affects the error bars. The lower mass and larger velocity of C ions result in a larger overlap of the error compared to silicon.

For silicon PKA cascades in SiC, the ratio of the electronic energy loss S_e to the nuclear energy loss S_n is 0.4 and 0.6, for 20 keV and 30 keV energy, respectively. This means that the nuclear energy loss is about twice the electronic energy loss, and therefore, the

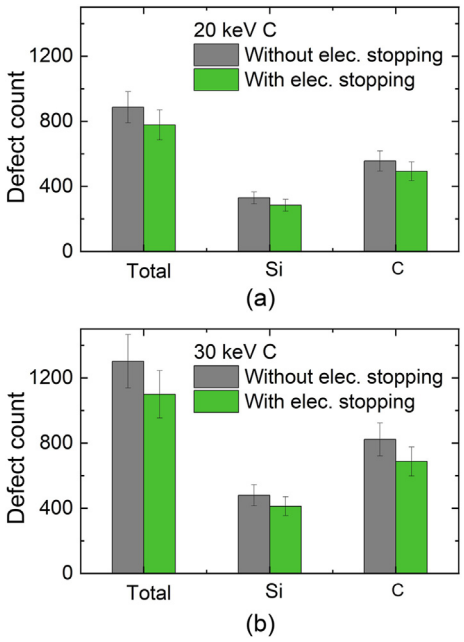

Fig. 3. Average number of defects as sum of interstitial and vacancies in (a) 20 keV C and (b) 30 keV C ion cascades in SiC. The total number of defects and the defects for each atom species are given for cascades with and without electronic stopping. The error bars represent the standard error over fifteen cascade events.

electronic stopping has a small or negligible effect on the number of surviving defects, as shown in Figs. 1 and 2. For carbon ions, the ratio of the electronic energy loss S_e to the nuclear energy loss S_n is 1.7 and 2.5, for 20 keV and 30 keV energy, respectively. Additionally, the mass of carbon is smaller than the mass of silicon, therefore the cut-off velocity $v_0 = \left(\frac{2E_0}{m}\right)^{1/2}$, where E_0 is the cut-off energy, is larger for the carbon ions. Because of this velocity-mass relationship for a given PKA energy, the C atoms, with smaller mass than the Si atoms, will have a larger velocity. Thus, for C atoms, we have both higher velocity and higher cut-off velocity compared to Si atoms. Therefore, the electronic stopping is more effective for carbon ions compared to silicon PKAs, resulting in a smaller number of defects when the electronic stopping is accounted for, as shown in Figs. 3 and 4.

Fig. 5 (a) and (b) show the size distribution of interstitial and vacancy cluster for 20 keV Si cascades in SiC, with and without the electronic stopping taken into account. Similarly, the interstitial

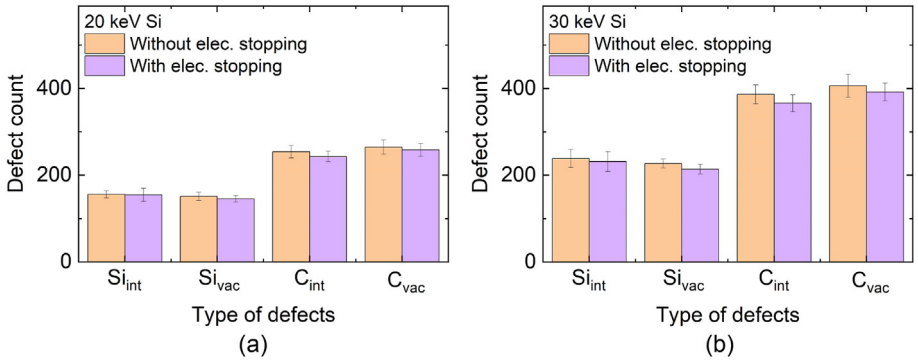

Fig. 2. Number of silicon interstitials and vacancies and carbon interstitial and vacancies in 20 keV Si and 30 keV Si cascades in SiC, with and without electronic stopping. The error bars represent the standard error over fifteen cascade events. (For interpretation of the references to colour in this figure legend, the reader is referred to the Web version of this article.)

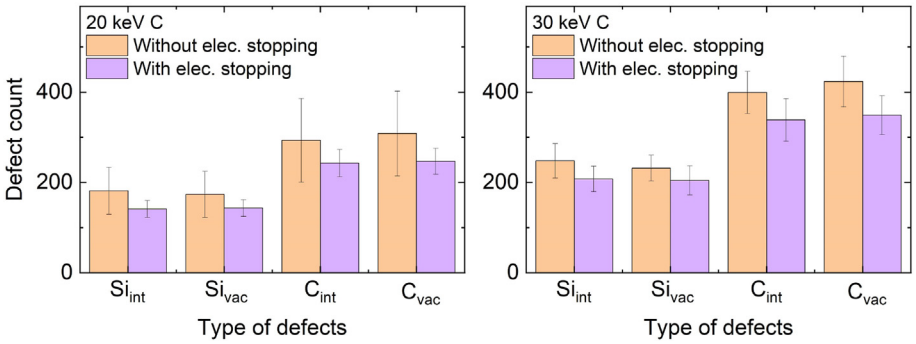

Fig. 4. Number of silicon interstitials and vacancies and carbon interstitial and vacancies in 20 keV C and 30 keV C cascades in SiC, with and without electronic stopping. The error bars represent the standard error over fifteen cascade events. (For interpretation of the references to colour in this figure legend, the reader is referred to the Web version of this article.)

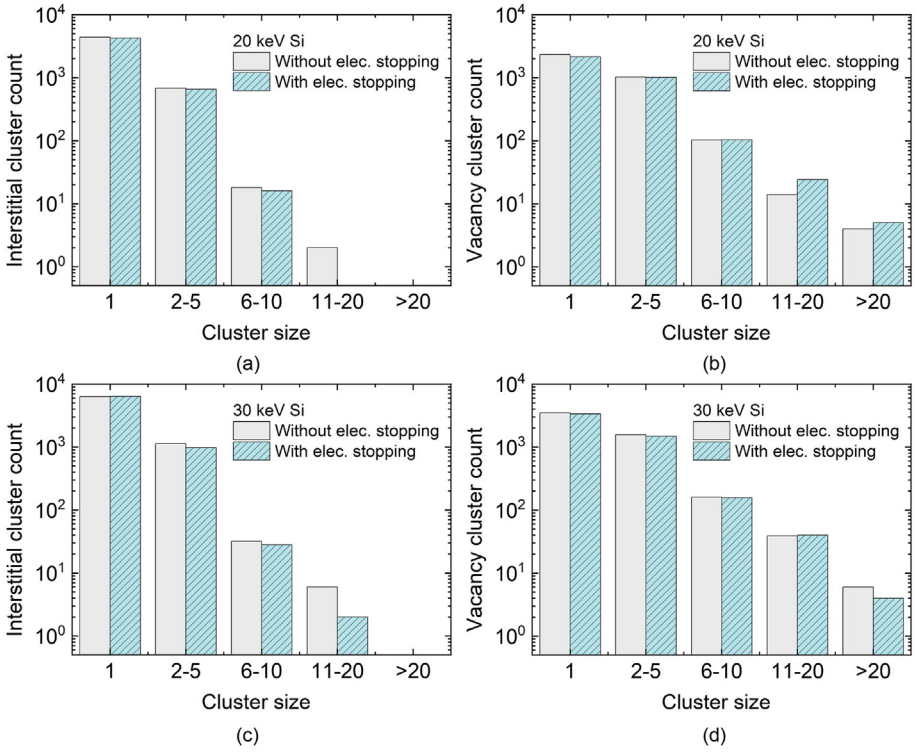

Fig. 5. (a) Interstitial and (b) vacancy cluster count in fifteen 20 keV Si ion cascades in SiC, with and without electronic stopping. (c) Interstitial and (d) vacancy cluster count in fifteen 30 keV Si ion cascades in SiC, with and without electronic stopping.

and vacancy cluster distribution for 30 keV Si ion cascades with and without electronic stopping are shown in Fig. 5 (c) and (d). Overall, a larger number of isolated interstitials than isolated vacancies are produced due to Si PKAs in SiC, and larger vacancy clusters are found than interstitial clusters, regardless of the electronic stopping. For Si PKA cascades, the number of single interstitials and single vacancies are not affected significantly by the electronic stopping, with a difference of about 1.6%−3.3%, and 7.6% for the isolated vacancies due to 20 keV Si PKAs. In the cascades where the electronic stopping is taken into account, the number of small and medium interstitial clusters and vacancy clusters is smaller than when the electronic stopping is ignored. For Si PKA cascades, the electronic stopping results in a smaller number of large clusters (except for the vacancy clusters due to 20 keV ions); however, larger clusters are found when the electronic stopping is ignored. The largest interstitial cluster found in 20 keV and 30 keV Si cascades consists of 13 and 19 interstitials, respectively, when the electronic stopping is not considered. When it is considered, the largest interstitial clusters found have sizes 10 and 14, for 20 keV and 30 keV Si, respectively. The sizes of the largest vacancy clusters found in cascades without the electronic stopping are 38 and 54, for 20 keV and 30 keV Si PKA energy, respectively. When the electronic stopping is active, the largest vacancy clusters consist of 28 and 35 vacancies, for 20 keV and 30 keV Si ion energy, respectively.

The interstitials and vacancy cluster distributions in fifteen cascades, with and without the electronic stopping and according to their size, for 20 keV C PKA in SiC are shown in Fig. 6 (a) and (b), and for 30 keV C ion in SiC, are shown in Fig. 6 (c) and (d). Similarly to the Si PKAs, more isolated interstitials are produced than isolated vacancies, for both energies, and larger vacancy clusters than

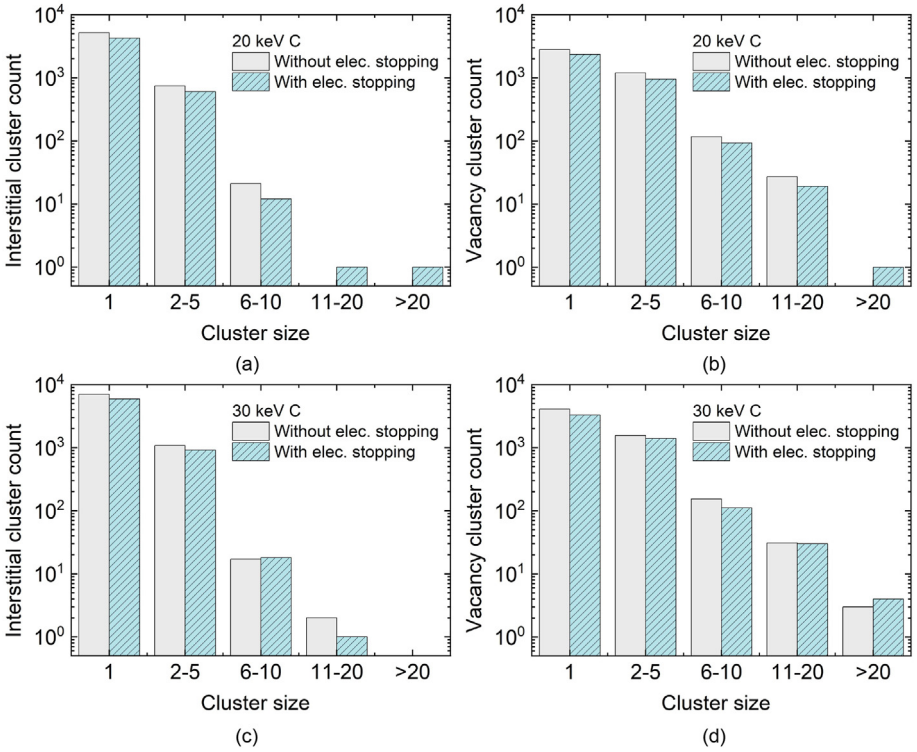

Fig. 6. (a) Interstitial and (b) vacancy cluster count in fifteen 20 keV C ion cascades in SiC, with and without electronic stopping. (c) Interstitial and (d) vacancy cluster count in fifteen 30 keV C ion cascades in SiC, with and without electronic stopping.

interstitial clusters are produced, regardless of the electronic stopping. When the electronic stopping is taken into account in the cascades, a smaller number of point defects is produced. The total numbers of isolated interstitials and isolated vacancies in 20 keV C cascades are 17.7% and 16.7% smaller when the electronic stopping is included. Similarly, for 30 keV C PKA energy, the numbers of isolated interstitial and isolated vacancies are 16% and 19.2% smaller when the electronic stopping is activated. Overall, a smaller number of small and medium size clusters are produced when the electronic stopping is included. When the electronic stopping is active, more large interstitial clusters are found in 20 keV C cascades and more large vacancy clusters are found for both energies.

Overall, the electronic stopping results in a smaller number of surviving defects, and the effect is more profound for the carbon defects. Additionally, the effects of the electronic stopping are more significant for the C PKA, and with increasing energy. For the C PKA, a smaller number of isolated defects are produced, and more large defect clusters are found. These findings indicate that the electronic stopping affects the defect production due to ion irradiation, and the ratio of the electronic energy loss S_e to the nuclear energy loss S_n is important for understanding the contribution of the electronic stopping to the damage production and defect cluster formation.

4. Conclusions

We performed molecular dynamics simulations of 20 keV and 30 keV Si and C PKAs in cubic SiC, with and without the electronic stopping taken into account. Our findings indicate that a smaller number of defects is produced when the electronic stopping is taken into account, particularly for C PKAs. We observe that larger vacancy clusters than interstitial clusters are formed for both energies, regardless of the electronic stopping. The effects of the electronic stopping is more profound for C PKAs, where the ratio of the electronic energy loss S_e to the nuclear energy loss S_n is 1.7 and 2.5 for 20 keV and 30 keV energy, respectively, which is more than four times larger than the corresponding ratio for 20 keV and 30 keV Si ions. In C cascades, when the electronic stopping is taken into account, a smaller number of single defects is formed, and a smaller number of small and medium size clusters and a larger number of large cluster are found. Overall, the results presented here indicate that the electronic stopping in intermediate energy ion irradiation can affect the response of the atomic structure to the energy deposition. In self-irradiation of SiC, the response of the microstructure to Si and C ions differs for the same energy, as they have different ratios of S_e/S_n, and different mass. This reveals that the ratio of S_e/S_n plays a role on the effects of the electronic stopping in the damage production under ion irradiation, as observed experimentally in Si ion irradiated SiC [46]. Further investigation of the effects of the electronic stopping on damage production in primary radiation damage in SiC is needed, such as for different energies and for overlapping events in order to understand its radiation response.

Funding

This manuscript has been authored by UT-Battelle, LLC under Contract No. DE-AC05-00OR22725 with the U.S. Department of Energy. The United States Government retains and the publisher, by accepting the article for publication, acknowledges that the United States Government retains a non-exclusive, paid-up, irrevocable, world-wide license to publish or reproduce the published form of this manuscript, or allow others to do so, for United States Government purposes. The Department of Energy will provide public access to these results of federally sponsored research in accordance with the DOE Public Access Plan (http://energy.gov/downloads/doe-public-access-plan).

Data availability

The raw/processed data required to reproduce these findings cannot be shared at this time as the data also forms part of an ongoing study.

CRediT authorship contribution statement

Eva Zarkadoula: Conceptualization, Methodology, Software, Formal analysis, Investigation, Writing - original draft, Writing - review & editing. **German Samolyuk:** Methodology, Writing - original draft, Writing - review & editing. **Yanwen Zhang:** Investigation, Writing - original draft, Writing - review & editing. **William J. Weber:** Conceptualization, Investigation, Writing - original draft, Writing - review & editing.

Declaration of competing interest

The authors declare that they have no known competing financial interests or personal relationships that could have appeared to influence the work reported in this paper.

Acknowledgment

EZ, YZ and WJW were supported by the U.S. Department of Energy, Office of Science, Basic Energy Sciences, Materials Sciences and Engineering Division. GDS was supported by the U.S. Department of Energy, Office of Science, Office of Fusion Energy Sciences, under Contract No. DE-AC05-00OR22725 with UT-Battelle LLC. This research used resources of the National Energy Research Scientific Computing Center, supported by the Office of Science, US Department of Energy under Contract No.DEAC02-05CH11231.

Appendix A. Supplementary data

Supplementary data to this article can be found online at https://doi.org/10.1016/j.jnucmat.2020.152371.

References

[1] S.J. Zinkle, V.A. Skuratov, D.T. Hoelzer, Nucl. Instrum. Methods Phys. Res. B 191 (2002) 758.
[2] A. Benyagoub, A. Audren, Nucl. Instrum. Methods Phys. Res. B 267 (2009) 1255.
[3] Y. Katoh, L.L. Snead, I. Szlufarska, W.J. Weber, Curr. Opin. Solid State Mater. Sci. 16 (2012) 143.
[4] S. Sorieul, X. Kerbiriou, J.-M. Costantini, L. Gosmain, G. Calas, C. Trautmann, J. Phys. Condens. Matter 24 (2012), 125801.
[5] Y. Zhang, H. Xue, E. Zarkadoula, M.A. Crespillo, F. Zhang, P. Liu, X. Wang, S. Zhang, T.-S. Wang, W.J. Weber, Curr. Opin. Solid State Mater. Sci. 21 (2017) 285.
[6] R. Devanathan, W. Weber, T. Diaz de la Rubia, Nucl. Instrum. Methods Phys. Res. Sect. B Beam Interact. Mater. Atoms 141 (1998) 118.
[7] F. Gao, W. Weber, Phys. Rev. B 63 (2000), 054101.
[8] R. Devanathan, W.J. Weber, F. Gao, J. Appl. Phys. 90 (2001) 2303.
[9] F. Gao, W.J. Weber, R. Devanathan, Nucl. Instrum. Methods Phys. Res. Sect. B Beam Interact. Mater. Atoms 180 (2001) 176.
[10] F. Gao, W.J. Weber, R. Devanathan, Nucl. Instrum. Methods Phys. Res. Sect. B Beam Interact. Mater. Atoms 191 (2002) 487.
[11] W.J. Weber, F. Gao, R. Devanathan, W. Jiang, C. Wang, Nucl. Instrum. Methods Phys. Res. Sect. B Beam Interact. Mater. Atoms 216 (2004) 25.
[12] C. Liu a, I. Szlufarska, J. Nucl. Mater. 509 (2018) 242.
[13] Y. Watanabe, K. Morishita, A. Kohyama, H.L. Heinisch, F. Gao, Nucl. Instrum. Methods Phys. Res. Sect. B Beam Interact. Mater. Atoms 267 (2009) 3223.
[14] D. Shrader, S.M. Khalil, T. Gerczak, T.R. Allen, A.J. Heim, I. Szlufarska, D. Morgan, J. Nucl. Mater. 408 (2011) 257.
[15] M.-J. Zheng, N. Swaminathan, D. Morgan, I. Szlufarska, Phys. Rev. B 88 (2013), 054105.
[16] J. Xi, P. Zhang, C. He, M. Zheng, H. Zang, D. Guo, L. Ma, Fusion Sci. Technol. 66 (2014) 235.
[17] H. Jiang, C. Jiang, D. Morgan, I. Szlufarska, Comput. Mater. Sci. 89 (2014) 182.
[18] K. Morishita, Y. Watanabe, A. Kohyama, H.L. Heinisch, F. Gao, J. Nucl. Mater. 386 – 388 (2009) 30.
[19] Y. Watanabe, K. Morishita, Y. Yamamoto, Nucl. Instrum. Methods Phys. Res. Sect. B Beam Interact. Mater. Atoms 269 (2011) 1698.
[20] N. Swaminathan, D. Morgan, I. Szlufarska, J. Nucl. Mater. 414 (2011) 431.
[21] E. Zarkadoula E, D.M. Duffy, K. Nordlund, M.A. Seaton, I.T. Todorov It, W.J. Weber, K. Trachenko, Electronic effects in high-energy radiation damage in tungsten, J. Phys. Condens. Matter 27 (2015), 135401.
[22] E. Zarkadoula, G. Samolyuk, H. Xue, H. Bei, W.J. Weber, Scripta Mater. 124 (2016) 6–10.
[23] E. Zarkadoula, G. Samolyuk, W.J.J. Weber, Alloys Compd 700 (2017) 106–112.
[24] E. Zarkadoula, G. Samolyuk, W.J. Weber, Scripta Mater. 138 (2017) 124–129.
[25] E. Zarkadoula, G. Samolyuk, W.J. Weber, AIP Adv. 8 (2018), 015121.
[26] E. Zarkadoula, G. Samolyuk, W.J. Weber, Mater. Res. Lett. 7 (12) (2019), 490.
[27] J.M. Pruneda, et al., Phys. Rev. Lett. 99 (2007), 235501.
[28] E. Artacho, J. Phys. Condens. Matter 19 (2007), 275211.
[29] J.M. Pruneda, D. Sanchez-Portal, A. Arnau, J.I. Juaristi, E. Artacho, Nucl. Instrum. Methods Phys. Res. B 267 (2009) 590–593.
[30] M.A. Zeb, J. Kohanoff, D. Sanchez-Portalde, E. Artacho, Nucl. Instrum. Methods Phys. Res. B 303 (2009) 59–61.
[31] R. Ullah, F. Corsetti, D. Sanchez-Portal, E. Artacho, Phys. Rev. B 91 (2015), 125203.
[32] E. Zarkadoula, R. Devanathan, W.J. Weber, M.A. Seaton, I.T. Todorov, K. Nordlund, M.T. Dove, K. Trachenko, High-energy radiation damage in zirconia: Modeling results, J. Appl. Phys. 115 (2014), 083507.
[33] S. Plimpton, J. Comp. Physiol. 117 (1995) 1–19.
[34] J. Tersoff, Phys. Rev. B 39 (1989) 5566.
[35] H. Huang, N.M. Ghoniem, J.K. Wong, M.I. Baskes, Model. Simulat. Mater. Sci. Eng. 3 (1995) 615.
[36] F. Gao, W.J. Weber, Nucl. Instrum. Methods Phys. Res. B 191 (2002) 504–508.
[37] J.F. Ziegler, J.P. Biersack, U. Littmark, The Stopping and Range of Ions in Matter, Pergamon, New York, 1985.
[38] G.D. Samolyuk, Y.N. Osetsky, R.E. Stoller, J. Nucl. Mater. 465 (2015) 83.
[39] D.W. Brenner, Phys. Rev. B 42 (1990) 15.
[40] D.M. Duffy, A.M.J. Rutherford, Phys. Condens. Matter 19 (2007), 016207.
[41] A.M. Rutherford, D.M. Duffy, J. Phys. Condens. Matter 19 (2007), 496201.
[42] Y. Zhong, K. Nordlund, M. Ghaly, R.S. Averback, Phys. Rev. B 58 (1998) 2361.
[43] E. Zhurkin, A. Kolesnikov, Atomic scale modelling of Al and Ni(111) surface erosion under cluster impact Nucl, Instr. Methods Phys. Res. Sect. B 202 (2003) 269–277.
[44] http://www.srim.org/.
[45] E. Zarkadoula, S.L. Daraszewic, D.M. Duffy, M.A. Seaton, I. Todorov, K. Nordlund, M.T. Dove, K. Trachenko, J. Phys. Condens. Matter 25 (12) (2013), 125402.
[46] H. Xue, Y. Zhang, W.J. Weber, Mater. Res. Lett. 5 (2017) 494–500.